JGR Solid Earth

RESEARCH ARTICLE
10.1029/2020JB019562

Volcano-Wide Deformation After the 2017 Erta Ale Dike Intrusion, Ethiopia, Observed With Radar Interferometry

Wenbin Xu[1,2], Lei Xie[3], Yosuke Aoki[4], Eleonora Rivalta[5], and Sigurjón Jónsson[6]

[1]School of Geosciences and Info-Physics, Central South University, Changsha, China, [2]Key Laboratory of Metallogenic Prediction of Nonferrous Metals and Geological Environment Monitoring, Ministry of Education, Central South University, Changsha, China, [3]Department of Land Surveying and Geo-Informatics, The Hong Kong Polytechnic University, Hong Kong, China, [4]Earthquake Research Institute, University of Tokyo, Tokyo, Japan, [5]GFZ German Research Centre for Geosciences, Potsdam, Germany, [6]Physical Science and Engineering Division, King Abdullah University of Science and Technology (KAUST), Thuwal, Saudi Arabia

Abstract Erta Ale Volcano erupted on 16 January 2017 in a difficult-to-access terrain in the Erta Ale volcanic range in Ethiopia. Like many other rifting ridge volcanoes, little is known about the properties of the deep magma plumbing system. Here, we analyze interferometric synthetic aperture radar data from different satellites between late January 2017 and May 2019 to study the ground deformation after the start of the intrusion to infer the possible geometry and volume change of the magma reservoir that fed the eruption. We identified volcano-wide subsidence of up to 9 cm and horizontal contraction of up to ~5 cm that extend from Erta Ale to neighboring volcanoes. The modeling results suggest that an off-rift NE-SW elongated mid-crustal source is required to explain the observed volcano-wide deformation, but the depth is poorly constrained and the shape is complex. We suggest the presence of vertical interactions between stacked mid-crustal magma sources. Our study demonstrates that a considerable volume of melt could have been stored in mid-crustal magma reservoirs within the slow-spreading Erta Ale Ridge to facilitate recent volcanic activity.

Key Points:
- We observe volcano-wide ground deformation following the 2017 Erta Ale dike intrusion using radar interferometry
- We model ground deformation after the intrusion between late January 2017 and May 2019 to study the properties of the magma plumbing system
- We find an off-rift NE-SW elongated mid-crustal source beneath Erta Ale with poorly constrained depth and a complex shape

Supporting Information:
- Supporting Information S1

Correspondence to:
W. Xu,
wenbin.xu@csu.edu.cn

Citation:
Xu, W., Xie, L., Aoki, Y., Rivalta, E., & Jónsson, S. (2020). Volcano-wide deformation after the 2017 Erta Ale dike intrusion, Ethiopia, observed with radar interferometry. *Journal of Geophysical Research: Solid Earth*, *125*, e2020JB019562. https://doi.org/10.1029/2020JB019562

Received 11 FEB 2020
Accepted 24 JUN 2020
Accepted article online 25 JUN 2020

1. Introduction

Volcanic eruptions and rifting events are often associated with ground deformation during both magma accumulation and erupting periods. Surface displacements during the later stages of an eruption are usually smaller in magnitude and rate than at the start of the eruption (Hamling et al., 2014; Hamlyn et al., 2014). If the deformation source is deep, the observed deformation is typically widespread and of small amplitude and thus sometimes difficult to detect. Nonetheless, leveling, tilt, GPS, and interferometric synthetic aperture radar (InSAR) observations have, in many cases, effectively captured the longer term response immediately after and between eruptions, yielding useful insights into the magma plumbing system and crustal rheology (e.g., Foulger et al., 1992; Hamling et al., 2014; Hamlyn et al., 2014, 2018; Tryggvason, 1984).

The southern Red Sea and the northern Afar regions have been exceptionally active during the past two decades, providing a good opportunity to study a variety of volcanic processes. The activity includes the 2005–2010 Manda Hararo-Dabbahu rifting episode (Grandin et al., 2010; Wright et al., 2006), the 2010–2011 Gulf of Aden earthquake swarm (Ahmed et al., 2016) and three volcanic eruptions in the southern Red Sea in 2007–2013 (Jónsson & Xu, 2015; Xu & Jónsson, 2014; Xu et al., 2015). Additionally, several volcanoes of the Afar-Danakil Rift in northern Ethiopia, where the spreading rate is ~16 mm/year in the N77°E direction, have also been recently active. Dallol Volcano erupted in 2004 (Nobile et al., 2012), Alu-Dalafilla Volcano in 2008 (Pagli et al., 2012), and Erta Ale Volcano in 2010 and 2017 (Field et al., 2012; Moore et al., 2019; Xu et al., 2017), respectively. While the preparatory phase and the early stage of these eruption events have been carefully studied, less attention has been paid to the later-stage deformation of these events. Here, we look into the deformation after the start of the 2017 dike intrusion in an attempt to improve our knowledge of the geometry, behavior, and physical properties of the magma plumbing system beneath the two summit calderas.

The crustal structure and magmatic and tectonic processes in the Erta Ale Rift have been studied since the 1970s and indicate the formation of a new oceanic crust within the Northern Danakil Depression

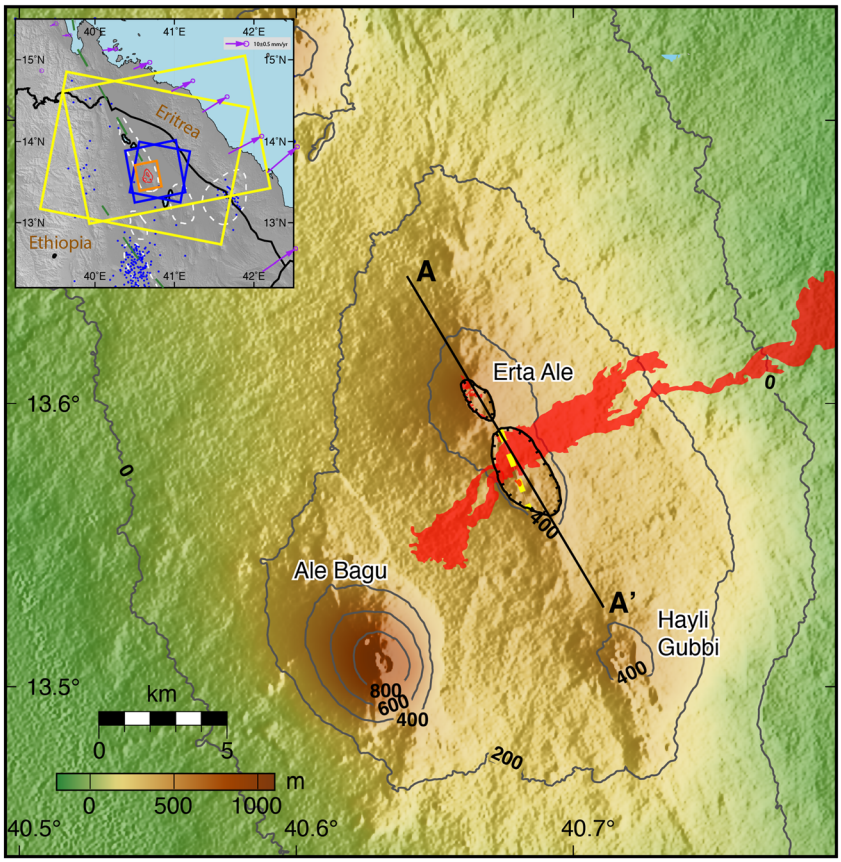

Figure 1. Topographic map of the Erta Ale volcanic complex, with the coverage of new lavas from January 2017 to March 2019 shown in red, the 2017 eruptive fissure in yellow and calderas outlined in black, respectively. Gray elevation contours have intervals of 200 m. Profile A-A′ represents the cross section shown in Figure 5. Inset shows yellow, blue, and orange boxes that outline SAR frames from the Sentinel-1 A/B, ALOS-2, and COSMO-SkyMed satellites, respectively. Blue dots show two decades of earthquakes from the National Earthquake Information Center catalog. Green dashed line marks the plate boundary in the region and purple arrows show GPS velocities with 95% confidence ellipses in a Eurasia-fixed reference frame (Viltres et al., 2020).

(Barberi & Varet, 1970; Doubre et al., 2007; Manighetti et al., 1998, 2001). The recent Erta Ale volcanic activity began when the lava lake within its northern caldera overflowed on 16 January 2017. This activity was followed by three fissure eruptions in the southern caldera (Moore et al., 2019; Xu et al., 2017). The eruptive fissures were soon reduced to cone-shaped vents depositing voluminous lavas within the southern caldera and down the eastern flank of the volcano. In our earlier study focusing on the early phase of the 2017 eruption and the associated deformation, we used InSAR data to constrain the shallow magma storage and transport at Erta Ale (Xu et al., 2017). We found that a vertical dike-shaped magma storage, situated beneath and feeding the lava lake, elongated into a shallow dike that fed the fissure eruptions in the southern caldera. A shallow horizontal reservoir was also found at a depth of ~1 km, hydraulically connected with this elongated dike. A further study showed that the lava lake level is sensitive to the pressure changes in the shallow plumbing system (Moore et al., 2019). The primary eruption was initially thought to have ceased in late January 2017, but the MOUNTS monitoring system (Valade et al., 2019) shows that fresh lava flowed out and deposited on the flank of the volcano until the late January 2020 without noticeable seismicity. This long-lasting eruptive activity indicates a continuing magma supply from a deeper source under the volcano.

Here, we present a series of ground deformation maps of Erta Ale Volcano from 30 January 2017 to 6 May 2019, using InSAR data acquired by three different radar satellite constellations (Figure 1) to study the deformation after the onset of the eruption. We use elastic dislocation models to represent possible magmatic

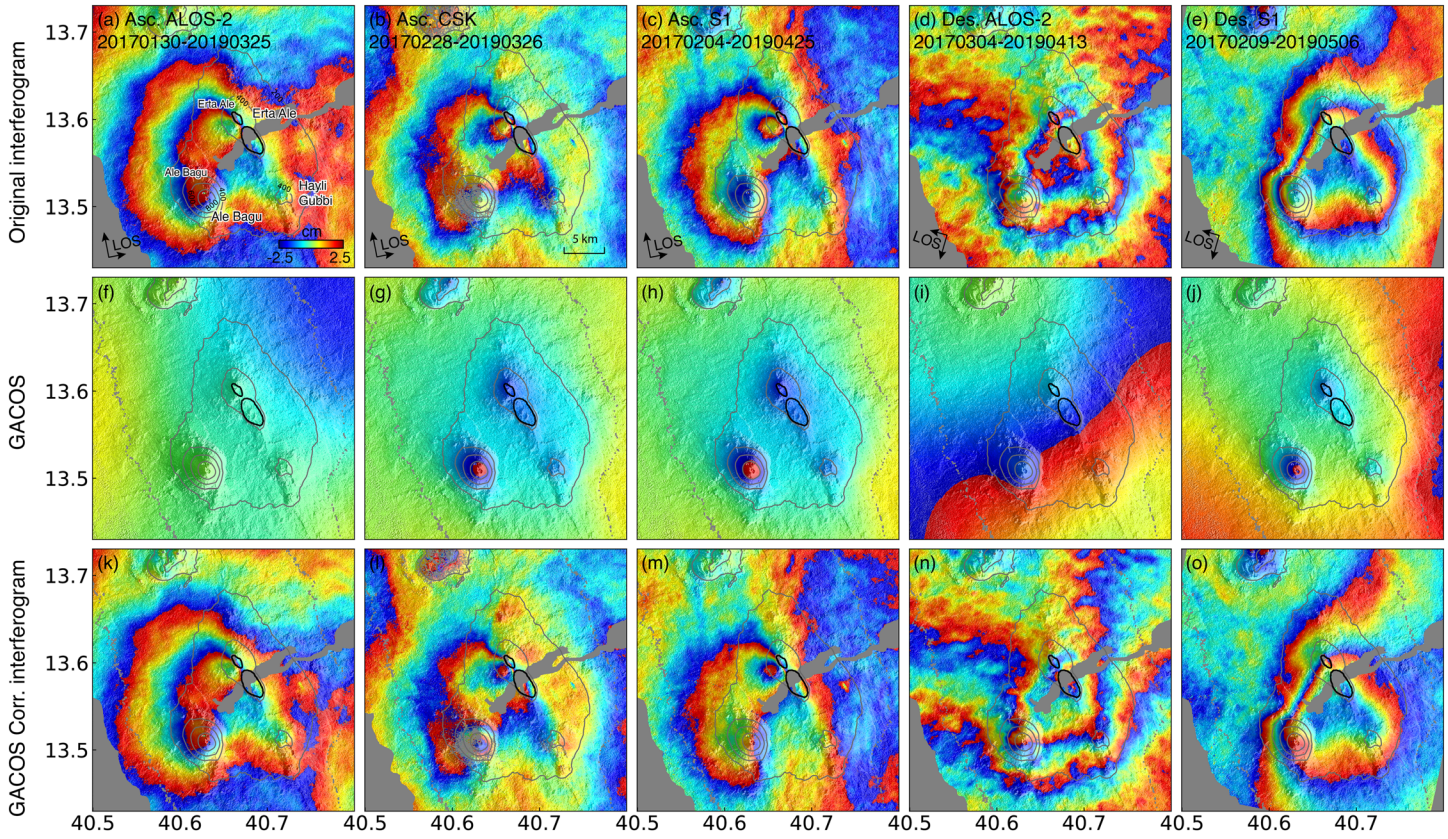

Figure 2. Atmospheric corrections of the InSAR data using the GACOS. (a–e) Original interferograms, (f–j) differenced wet delay maps along the LOS direction derived from GACOS, and (k–o) corrected interferograms. Note that the interferograms were unwrapped and then rewrapped at a 5-cm LOS displacement per fringe.

sources experiencing pressure changes in the subsurface to explain the observed deformation. Finally, we discuss the implications of the results regarding the magma storage system under Erta Ale Volcano.

2. InSAR Data Processing and Inversion Methods

We used SAR data from the Sentinel-1 A/B, ALOS-2, and COSMO-SkyMed satellites (Table S1 in the supporting information) and produced interferograms with the InSAR Scientific Computing Environment (ISCE) software using the two-pass differential InSAR technique (Agram et al., 2016; Rosen et al., 2012). Two different processing chains (stripmapApp and topsApp) were applied for the different satellite acquisition modes. Because the ALOS-2 and COSMO-SkyMed data are conventional stripmap data, we directly coregistered the SAR images using information about the acquisition geometry and the 1 arc-sec SRTM DEM of the area (Farr et al., 2007), accounting for inaccurate orbits and topography with further geometrical coregistration. The Sentinel-1 A/B data were collected in the Terrain Observation by Progressive Scan (TOPS) mode, which requires more advanced image coregistration method. Therefore, we applied the enhanced spectral diversity method (Fattahi et al., 2017) following the initial conventional image coregistration. We then multilooked the resulting interferograms (i.e., Sentinel-1 20 × 4, ALOS-2 12 × 20, and CSK 10 × 10 in the range and azimuth directions) and used the SRTM DEM to remove the topographic contribution. Finally, we further suppressed the signal noise with a power spectral filter (Goldstein & Werner, 1998) and used the minimum-cost flow network algorithm for the phase unwrapping (Chen & Zebker, 2002) to yield the final unwrapped interferograms (Figures 2a–2e).

We used the Generic Atmospheric Correction Online Service for InSAR (GACOS) to reduce atmospheric signals in our interferograms providing tropospheric delay maps estimated from the European Center for Medium-range Weather Forecasts (ECMWF) and GPS observations (Yu et al., 2017). We differenced the GACOS zenith total delay maps that correspond to our interferograms, projected them into the line of

sight (LOS) direction, and then resampled the result to match the interferogram posting. The GACOS corrections indicate that atmospheric signals are not strong in this dry region (Figures 2f–2j) and have a limited impact on the interferograms (Figures 2k–2o). The GACOS correction fails to capture the strongest atmospheric signals, which are easily identified in the interferograms (Figures 2n and 2o). The apparent topography-related atmospheric signal at Ale Bagu Volcano in the ascending COSMO-SkyMed (Figure 2g) and Sentinel-1 data (Figure 2h), for example, is not captured by the GACOS correction in the ALOS-2 data (Figure 2f). We then masked out the deforming area from the GACOS-corrected interferograms and fitted the plane to these data to reduce the remaining atmospheric gradients (Figures 2k–2o). The remaining uncorrected signals are mainly associated with atmospheric turbulence.

As suggested by the observed deformation pattern, we think that two major sources of ground deformation were active during the 2 years following the onset of the eruption, that is, a deeper source causing the volcano-wide deformation and a shallower dike-like source responsible for the deformation close to the northern caldera. To examine this, we first used quadtree subsampling of the LOS displacements to reduce the data size without significant loss of information (Jónsson & Xu, 2015), and we then estimated the optimal source model parameters that best match to the observations using an elastic half-space with a Poisson's ratio of 0.25. Data variances of the five interferograms were used as relative observation weights in the source parameter estimation. We did not include effects of topography in the modeling (Williams & Wadge, 2000), although they may broaden the predicted deformation; these effects have been found to be secondary in the case of Erta Ale (Xu et al., 2017).

Volcano deformation is typically modeled with planar or spherical pressure sources (Segall, 2010). The planar model (Okada, 1985) is effective in studying the deformation field resulting from magmatic intrusions in the form of dikes or sills (Amelung et al., 2000; Xu et al., 2016), but it is limited by artifact singularities because of the lack of full rotational degrees of freedom (Okada, 1985). Nikkhoo et al. (2017) developed a generalized source model of pressurized cavities, namely, the compound dislocation model (CDM), which uses a set of three mutually orthogonal rectangular dislocations that are free to dip in any direction, representing planar and volumetric sources of any aspect ratios. Therefore, we carried out model parameter estimations using two different source models. The first model includes one CDM source (CDM source, that is, three perpendicular tensile dislocations; Nikkhoo et al., 2017), to represent the deeper source and one rectangular dislocation (Okada, 1985) to represent the shallow dike source (Model I). The CDM source consists of 10 parameters: centroid location (λ_0, ϕ_0, d), rotation angles (ω_x, ω_y, ω_z), semiaxes (a, b, c), and uniform opening or closing (u). Because we do not have a prior knowledge about the deep source, we set wide bounds on the possible source parameters of the CDM. For the shallow dike source, we set the location and orientation in our previous study (Xu et al., 2017) and estimated the dip angle, geometry, and uniform closing value. We also sought to explain the observed deformation with a combination of a horizontal sill, representing the deeper source and a dike (Model II). We used a horizontal rectangular dislocation (Okada, 1985) to represent the sill, solving for location (λ_0, ϕ_0), geometry (l, w), depth, and closure (u), and modeled the shallow dike as before. A nonlinear simulated annealing estimation algorithm (Cervelli et al., 2001) was used to find the best fitting model parameters, and a randomize-then-optimize method (500 times) was applied to assess the model parameter uncertainties (Bardsley et al., 2014; Xu et al., 2016).

3. Results

The atmosphere-corrected three ascending and two descending interferograms that we use span more than 2 years after the eruption began. These interferograms consistently indicate an approximately 20-km broad volcano-wide subsidence, suggesting contraction of a subhorizontal deep source (Figures 3a–3e). The smaller asymmetric deformation signal, located just southwest of the northern caldera, is common to only the ascending interferograms and shows an LOS range increase of ~10 cm. This deformation might be caused by contraction of the dike intrusion identified in data from the onset of the eruption in 2017 (Xu et al., 2017). The white gaps in the interferograms are related to the deposition of lava flow that extends ~16 km to the east from the southern caldera (Figure 3).

We combined all the interferograms to estimate the near east-west horizontal and vertical displacements. The resulting east-west displacement map is dominated by two displacement lobes, indicating that the ground moved toward the northern caldera of Erta Ale and Ale Bagu (Figures 4a–4d). The large

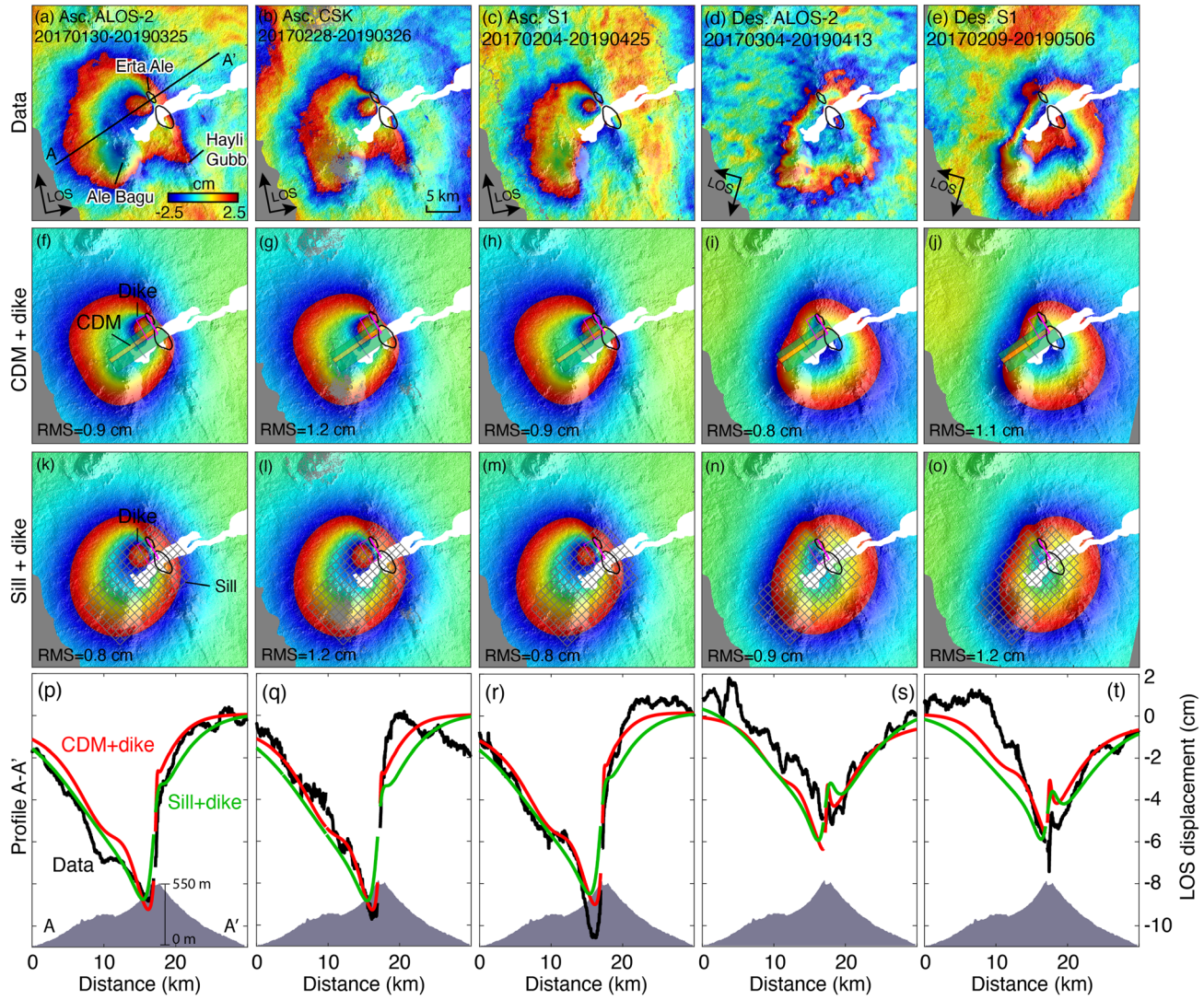

Figure 3. GACOS + atmosphere gradient corrected InSAR data indicating subsidence for approximately 2 years after the onset of the Erta Ale dike intrusion in comparison with the model prediction results. (a–e) Five unwrapped and then rewrapped interferograms at 5-cm LOS displacement per fringe. The Erta Ale calderas are shown with black lines and new lavas are in white. (f–j) CDM + dike model predictions, with the surface projections of the geometrical structure of CDM in green and the dike in purple. (k–o) Sill + dike model predictions with the surface projections of the distributed-closure sill model in gray and the dike in purple. (p–t) Observed (black) and modeled displacements using the CDM + dike model (red) and the sill + dike model (green) along profile A-A', with negative LOS displacement defined as increase in range because of subsidence. The shaded area shows the profile topography.

horizontal surface displacements (Figure 4d) and land subsidence (Figures 4e–4h) extending from Ale Bagu to Erta Ale and Hayli Gubb indicate that a deep source is deflating under the area. The maximum horizontal and vertical displacements of ~6 and 9 cm are observed near the northern caldera suggesting they are mainly caused by the contraction of a shallow dike. As more subsidence is found to the southwest of Erta Ale, than on the other side of the caldera, that deep source is likely offset to the southwest of the calderas.

Our best fitting model shows that the CDM predictions fit well with the observed volcano-wide deformation (Figures 3 and S1). Similarity, the observed deformation near the northern caldera is well matched by the rectangular dislocation model representing the dike (Figure S2). The center of the CDM source is located on the western flank of Erta Ale Volcano, about 3 km away from the northern caldera. However, its depth is not well constrained and ranges from 4 to 11 km (Figure 5a). The minimum axis and intermediate axis to maximum axis ratios for the best fitting CDM source are 0.38 and 0.67, respectively. We also calculated the eigenvalues (M1, M2, and M3 with $M1 \geq M2 \geq M3$) of the optimal CDM moment tensor, yielding eigenvalue ratios of $M2/M1 = 0.68$ and $M3/M1 = 0.78$, which correspond to a point falling within the ellipsoid domain

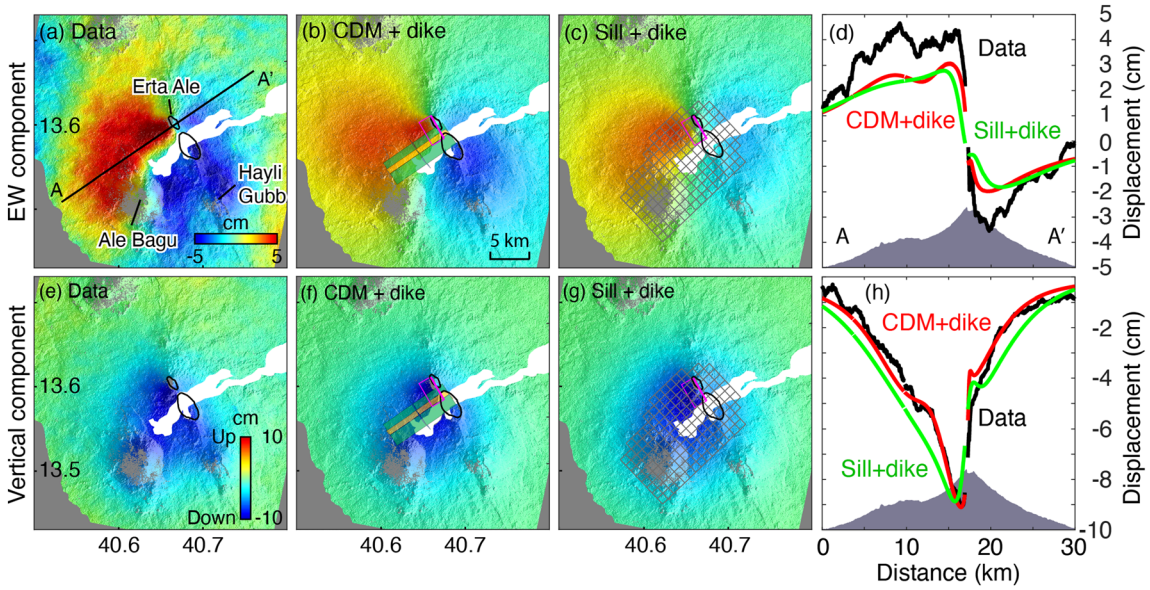

Figure 4. Observed and modeled (first row) EW horizontal and (second row) vertical displacement fields. (a) The observed, (b) the modeled EW horizontal component of deformation from CDM + dike model, and (c) sill + dike model predictions, respectively. Positive values indicate eastward movement. The surface projections of the geometrical structure of CDM are in green, while the sill and the dike are in purple. (d) Observed (black) and modeled horizontal displacements using the CDM + dike model (red) and the sill + dike model (green) along profile A-A'. The shaded area shows the topography profile. Figures in the second row show the vertical component of deformation. Negative deformation indicates subsidence.

(Nikkhoo et al., 2017). If the uncertainties of the model parameters are considered, then the deforming source fits within the CDM domain (Figures 5b and S3). Using the best fitting CDM model parameters, we found that the potency (volume of magma extracted from the reservoir, which is generally larger than the volume change of the reservoir depending on the rock bulk modulus and reservoir shape) is about -0.035 km^3. The top of the best fitting dike is located at a depth of 0.3 km and dips 60° to the southwest, connecting to the top of CDM source (Table S2). The average closure value of this shallow dike is ~10 cm resulting in a minimal volume decrease of 0.001 km^3. The RMS of the residuals is approximately 1 cm for the different

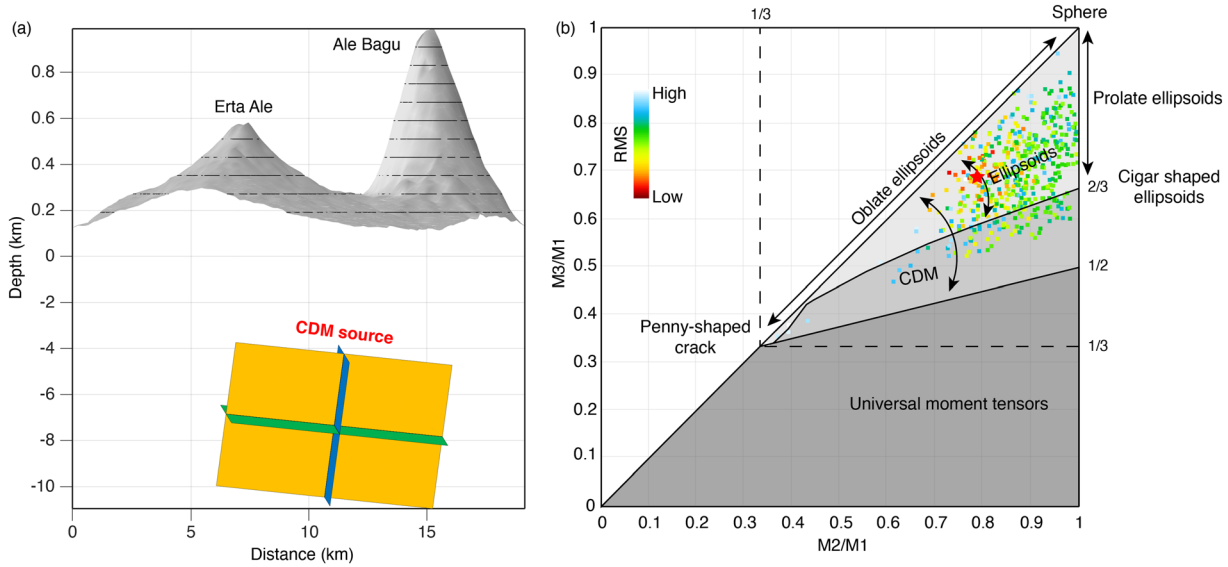

Figure 5. The best fitting compound dislocation model (CDM) and the uncertainty of the eigenvalue ratio distribution. (a) Perspective view from N30°W of the best fitting CDM source with topographic contours on Erta Ale and Ale Bagu at 100-m intervals. (b) RMS distribution of the eigenvalue ratios of the CDM source overlain on the eigenvalue ratios. Red star represents the optimal eigenvalue ratio. The figure was constructed after Nikkhoo et al. (2017).

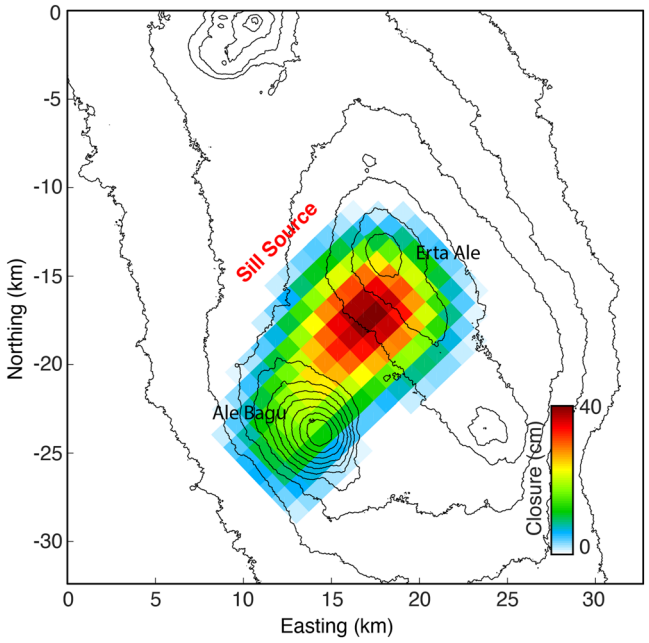

Figure 6. Plan view of the estimated spatially variable sill closure overlain by topographic contours (100-m intervals).

InSAR data, suggesting that the CDM + dike model adequately reproduces the observed deformation signals (Figures 3, 4, and S4).

The nonlinear estimation of model II yields a sill with a depth of ~11 km, corresponding to the bottom of the estimated CDM source but with an unrealistically narrow width of ~3 km. To construct a more reasonable sill closure model, we enlarged the dimensions of the sill to 20 km × 20 km, discretized it into 400 rectangular 1 km × 1 km patches and estimated spatially variable sill contraction. The results show up to ~0.3 m of sill closure, peaking ~3 km southwest of the northern caldera, with the orientation of the sill consistent with the CDM source (Figure 6). The estimated volume change of the deep sill is −0.024 km^3. This sill + dike model explains the observed deformation just as well as the CDM + dike model as demonstrated by the similar root mean square (RMS) values (Figures 3k–3o, S4, and S5). The trade-offs between the different model parameters are significant in both cases (Figures S1–S3); uncertainties indicate that the location and orientation of the mid-crustal source are well constrained, whereas the shape and depth are not (Figure S6). Therefore, we deem the shape of the deformation source to be complex and possibly much thicker than a sill or consisting of multiple elongated lenses (Figure 7).

4. Discussion

Our analysis of the ~2 years of deformation of Erta Ale Volcano, after the onset of the eruption that started on 16 January 2017, indicates a sizeable mid-crustal magma storage system ranging from a depth of ~4 to ~11 km. This is in accordance with the thin estimated effective elastic plate thickness (5 km) in the region (Hayward & Ebinger, 1996). The 2004 Dallol intrusion, at the northern edge of the Erta Ale Ridge, showed that the intruded dike was sourced from an approximately 6-km depth (Nobile et al., 2012). Similarly, a 5-month seismological experiment in the Asal Ghoubbet Rift showed that the magma reservoir was located at a depth greater than 5 km (Doubre et al., 2007). These studies suggest that the magma plumbing system of the rift-axis volcanoes of the Erta Ale Ridge has somewhat deeper magma chambers than those of the Krafla (Árnadóttir et al., 1998) and Galápagos volcanoes (Amelung et al., 2000). However, like the rift-axis, the center of the deep reservoir is located beneath the western flank of Erta Ale Volcano and is not oriented in the NNW-EES direction. A magnetotelluric survey found a similar large magma reservoir offset to the west of the rifted region in the

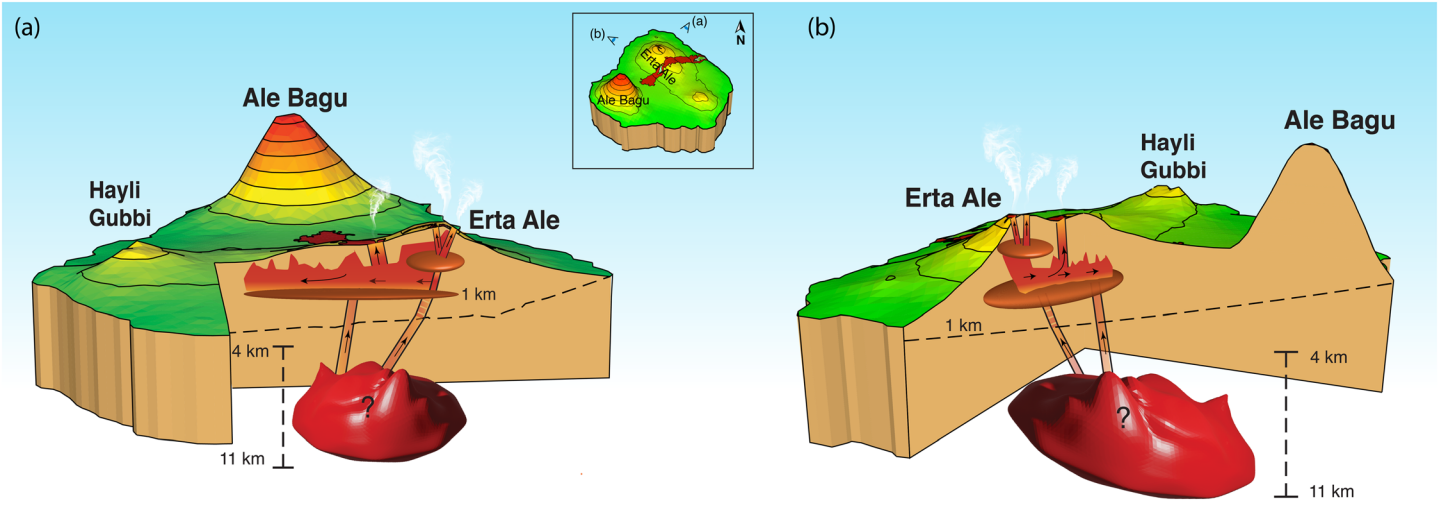

Figure 7. A schematic cartoon showing the inferred magma plumbing system of Erta Ale Volcano viewing from the (a) northeast and (b) northwest side of the volcano, respectively. The figure is not to scale.

Dabbahu magmatic segment (Desissa et al., 2013). The deep chamber under Erta Ale seems to extend to the neighboring Ale Bagu Volcano, suggesting a possible deep link between the two magmatic systems. The existing petrological and geochemical studies show that the Erta Ale and Ale Bagu basalts have similar $^{87}Sr/^{86}Sr$ and $^{143}Nd/^{144}Nd$ ratios suggesting that they originated from a single reservoir, prevalent mantle (PREMA), which is commonly called the hot mantle plume (Hagos et al., 2016). Hagos et al. (2016) found that the Ale Bagu basalts are derived from a deeper magma chamber than those of the Erta Ale, which was consistent with our modeling results. Other evidence of connected reservoirs were found at the Erta Ale Ridge in the case of the 2008 Alu-Dalafilla Eruption, where analysis and modeling of InSAR data revealed multiple laterally connected deformation sources at depth (Pagli et al., 2012) and in the 2010 Eyjafjallajökull Eruption, where study of InSAR data and earthquake locations showed a "stacked" magmatic system at depths between 4 and 6 km (Sigmundsson et al., 2010; Tarasewicz et al., 2012).

Erta Ale is the most active volcano of the Erta Ale Ridge. From recent activity from 2004 to 2019, we found that the volcanic eruption characteristics at Erta Ale can be divided into three phases: (1) pre-eruption shallow dike inflation in the northern caldera, (2) lava lake overspilling and fissure opening (Field et al., 2012; Xu et al., 2017), and (3) early co-eruptive shallow magma source inflation, followed by a long-lasting subsidence due to deep magmatic source deflation. In the first stage, obvious ground deformation was observed prior to the 2010 and 2017 eruptions (Barnie et al., 2016; Moore et al., 2019; Xu et al., 2017) and was associated with inflation of a shallow approximately 3-km-long dike prior to the eruptions that fed the lava lake. In the second stage, the 2010 eruption was characterized by Strombolian activity, but the 2017 eruption produced voluminous lava flows and obvious ground deformation (Xu et al., 2017). Both eruptions seem to have been fed from a common shallow reservoir (Field et al., 2012; Moore et al., 2019; Xu et al., 2017). Modeling of the observed ground deformation associated with the onset of the 2017 eruption suggests that the shallow magma system involves an interaction of multiple melt lenses (Xu et al., 2017). In the third stage, the early co-eruptive shallow magma source inflation can possibly be attributed to the refilling of a shallow reservoir in response to additional magma inflow. The shallow magma chamber temporarily stores the recharged magma, whereas the later-stage eruptive subsidence shows evidence for additional mixing from a deeper level, probably from the primary magmatic system that stores a large volume of magma (Figure 6). The shallow dike is always active during all periods, inflating prior to eruptions and contracting during and after eruptions, possibly to accommodate the magma reservoir pressure changes and lava lake level variations.

Based on our modeling estimation results, approximately 0.035 km^3 of magma was drawn from the deep magmatic reservoir during the 2 years after the onset of the 2017 eruption. The volume of withdrawn magma is nearly 5–6 times larger than that erupted in the 2010 (0.006 km^3) eruption and in the initial phase of the 2017 (0.007 km^3) eruption (Field et al., 2012; Xu et al., 2017). Previous studies have shown that the rate of shallow magma accumulation is ~0.002 km^3/year (Barnie et al., 2016; Xu et al., 2017). The erupted magma during the first 2 years after the onset of eruptive activity in 2017 is thus equivalent to 17 years of magma accumulation. To roughly estimate the thickness of the lava deposited during the past 2 years, we mapped decorrelated areas from the ascending ALOS-2 interferogram and found that the surface lava coverage is ~28 km^2. Assume that the entire magma volume of ~0.035 km^3 was deposited at the surface and without considering exsolved volatiles in the magma (Rivalta & Segall, 2008), yielding an average lava flow thickness of ~1.4 m. This estimation is within the range of 0.5–2.5 m found by Moore et al. (2019).

The parameters of deep magmatic sources obtained from estimations using space geodetic data are often affected by large uncertainties (Hamlyn et al., 2014; Lundgren et al., 2015; Xu et al., 2016). However, both the CDM + dike and sill + dike models match the vertical displacements well but underestimate the horizontal displacements (Figure S5). This is possibly because the near-polar orbits and steep look angles make the radar satellites more sensitive to vertical than to horizontal movements. The presence of atmospheric signals in the data, especially in descending orbits (Figures 3s, 3t, S4), could also bias the model results, as the deformation signals are not strong (only ~9 cm). Therefore, the detailed structure of deep sources is often poorly resolved. Our modeling shows that both a large deflating CDM source, extending from a depth of 4–11 km, and a deep sill (11 km depth) can explain the data well. The CDM source has 10 model parameters, whereas the discretized sill source has over 400 model parameters. A more complex system of stacked sources could probably produce similar ground deformation (e.g., Amoruso & Crescentini, 2013), making it impossible to distinguish between these models based on the space geodetic data alone. Similarly,

Hamlyn et al. (2014) showed that both a Mogi source (7-km depth) and a sill source (11-km depth) could fit the observed ground deformation following the 2011 Nabro Eruption, although the Mogi source (Mogi, 1958) provided a slightly better fit and was selected as the preferred deep source model. Illsley-Kemp et al. (2018) found the existence of a sill-like magma chamber at an approximate depth of 12 km below Alu-Dalafilla, a volcano located within the Erta Ale Rift. This is remarkably similar to the best fit depths for our estimated sill or CDM sources. Additionally, the deep magma reservoir of Nevado del Ruiz Volcano was found to be well modeled by either a point or spherical source from InSAR data (Lundgren et al., 2015). Together, these findings indicate that it remains challenging to fully resolve the parameters of deep magmatic sources from InSAR observations alone using simple analytic models. Inhomogeneities in the source geometry and in the structure and rheology of the crust of the Earth lead to biased model parameters and introduce model parameter uncertainties; however, these effects are difficult to quantify.

5. Conclusions

From the InSAR data of three different satellites, we have presented a consistent subsidence pattern at Erta Ale Volcano, observed after the onset of the 2017 eruption, of up to 9 cm from 2017 to early 2019. The observed subsidence and modeling results suggest the depressurization of vertically stacked magma sources from a depth of 4–11 km, primarily because of magma withdrawal to the surface. From these results and the inferred shallow magmatic plumbing system of earlier studies (Moore et al., 2019; Xu et al., 2017), we suggest that magma under Erta Ale is stored in multiple hydraulically connected melt lenses at different depths.

Data Availability Statement

Sentinel-1 SAR images were downloaded from the Sentinel-1 Scientific Data Hub (https://scihub.copernicus.eu). ALOS-2 SAR images were provided by the Japan Aerospace Exploration Agency (ER2A2N016, ER2A2N161, http://en.alos-pasco.com/). CSK data were found from e-geos (http://213.215.135.195). The processed InSAR data are available at https://github.com/Wenbin16/Erta-Ale-2017-eruption.

Acknowledgments
We thank the Editor, the Associate Editor, and the two reviewers for their constructive comments that helped us to improve our manuscript. The research was supported by the National Natural Science Foundation of China under Grant 41804015 and by the National Key R&D Program of China (2019YFC1509205).

References

Agram, P. S., Gurrola, E. M., Lavalle, M., Sacco, G. F., & Rosen, P. A. (2016). *The InSAR Scientific Computing Environment (ISCE): An Earth science SAR processing framework, toolbox, and foundry*. Paper presented at AGU Fall Meeting in San Francisco.

Ahmed, A., Doubre, C., Leroy, S., Kassim, M., Keir, D., Abayazid, A., et al. (2016). Seafloor spreading event in western Gulf of Aden during the November 2010–March 2011 period captured by regional seismic networks: Evidence for diking events and interactions with a nascent transform zone. *Geophysical Journal International*, *205*(2), 1244–1266. https://doi.org/10.1093/gji/ggw068

Amelung, F., Jónsson, S., Zebker, H., & Segall, P. (2000). Widespread uplift and 'trap-door' faulting on Galápagos volcanoes observed with radar interferometry. *Nature*, *407*(6807), 993–996. https://doi.org/10.1038/35039604

Amoruso, A., & Crescentini, L. (2013). Analytical models of volcanic ellipsoidal expansion sources. *Annales de Geophysique*, *56*, S0435. https://doi.org/10.4401/ag-6441

Árnadóttir, T., Sigmundsson, F., & Delaney, P. T. (1998). Sources of crustal deformation associated with the Krafla, Iceland, eruption of September 1984. *Geophysical Research Letters*, *25*(7), 1043–1046. https://doi.org/10.1029/98GL50655

Barberi, F., & Varet, J. (1970). The Erta Ale volcanic range (Danakil depression, northern Afar, Ethiopia). *Bulletin of Volcanology*, *34*(4), 848–917. https://doi.org/10.1007/BF02596805

Bardsley, J. M., Solonen, A., Haario, H., & Laine, M. (2014). Randomize-then-optimize: A method for sampling from posterior distributions in nonlinear inverse problems. *SIAM Journal on Scientific Computing*, *36*(4), A1895–A1910. https://doi.org/10.1137/140964023

Barnie, T. D., Oppenheimer, C., & Pagli, C. (2016). Does the lava lake of Erta Ale Volcano respond to regional magmatic and tectonic events? An investigation using Earth observation data. *Geological Society, London, Special Publications*, *420*(1), 181–208. https://doi.org/10.1144/SP420.15

Cervelli, P., Murray, M. H., Segall, P., Aoki, Y., & Kato, T. (2001). Estimating source parameters from deformation data, with an application to the March 1997 earthquake swarm off the Izu Peninsula, Japan. *Journal of Geophysical Research*, *106*(B6), 11,217–11,237. https://doi.org/10.1029/2000JB900399

Chen, C. W., & Zebker, H. A. (2002). Phase unwrapping for large SAR interferograms: Statistical segmentation and generalized network models. *IEEE Transactions on Geoscience and Remote Sensing*, *40*(8), 1709–1719. https://doi.org/10.1109/TGRS.2002.802453

Desissa, M., Johnson, N. E., Whaler, K. A., Hautot, S., Fisseha, S., & Dawes, G. (2013). Mantle magma reservoir imaged magnetotellurically beneath the proto-mid-ocean ridge in Afar, Ethiopia. *Nature Geoscience*, *6*(10), 861–865. https://doi.org/10.1038/ngeo1925

Doubre, C., Manighetti, I., Dorbath, C., Dorbath, L., Jacques, E., & Delmond, J.-C. (2007). Crustal structure and magmato-tectonic processes in an active rift (Asal-Ghoubbet, Afar, East Africa): 1. Insights from a 5-month seismological experiment. *Journal of Geophysical Research*, *112*(B11), B05405. https://doi.org/10.1029/2005JB003940

Farr, T. G., Rosen, P. A., Caro, E., Crippen, R., Duren, R., Hensley, S., et al. (2007). The shuttle radar topography mission. *Reviews of Geophysics*, *45*, RG2004. https://doi.org/10.1029/2005RG000183

Fattahi, H., Agram, P., & Simons, M. (2017). A Network-Based Enhanced Spectral Diversity Approach for TOPS Time-Series Analysis. *IEEE Transactions on Geoscience and Remote Sensing*, *55*(2), 777–786. https://doi.org/10.1109/tgrs.2016.2614925

Field, L., Barnie, T., Blundy, J., Brooker, R. A., Keir, D., Lewi, E., & Saunders, K. (2012). Integrated field, satellite and petrological observations of the November 2012 eruption of Erta Ale. *Bulletin of Volcanology*, *74*, 2251–2271. https://doi.org/10.1007/s00445-012-0660-7

Foulger, G. R., Jahn, C.-H., Seeber, G., Einarsson, P., Julian, B. R., & Heki, K. (1992). Post-rifting stress relaxation at the divergent plate boundary in Northeast Iceland. *Nature*, *358*(6386), 488–490. https://doi.org/10.1038/358488a0

Goldstein, R. M., & Werner, C. L. (1998). Radar interferogram filtering for geophysical applications. *Geophysical Research Letters*, *25*(21), 4035–4038. https://doi.org/10.1029/1998GL900033

Grandin, R., Socquet, A., Jacques, E., Mazzoni, N., de Chabalier, J. B., & King, G. C. P. (2010). Sequence of rifting in Afar, Manda-Hararo rift, Ethiopia, 2005–2009: Time-space evolution and interactions between dikes from interferometric synthetic aperture radar and static stress change modeling. *Journal of Geophysical Research*, *115*, B10413. https://doi.org/10.1029/2009JB000815

Hagos, M., Koeberl, C., & van Wyk de Vries, B. (2016). The Quaternary volcanic rocks of the northern Afar Depression (northern Ethiopia): Perspectives on petrology, geochemistry, and tectonics. *Journal of African Earth Sciences*, *117*, 29–47. https://doi.org/10.1016/j.jafrearsci.2015.11.022

Hamling, I. J., Wright, T. J., Calais, E., Lewi, E., & Fukahata, Y. (2014). InSAR observations of post-rifting deformation around the Dabbahu rift segment, Afar, Ethiopia. *Geophysical Journal International*, *197*(1), 33–49. https://doi.org/10.1093/gji/ggu003

Hamlyn, J., Wright, T., Walters, R., Pagli, C., Sansosti, E., Casu, F., et al. (2018). What causes subsidence following the 2011 eruption at Nabro (Eritrea)? *Progress in Earth and Planetary Science*, *5*(1), 31. https://doi.org/10.1186/s40645-018-0186-5

Hamlyn, J. E., Keir, D., Wright, T. J., Neuberg, J. W., Goitom, B., Hammond, J. O. S., et al. (2014). Seismicity and subsidence following the 2011 Nabro Eruption, Eritrea: Insights into the plumbing system of an off-rift volcano. *Journal of Geophysical Research: Solid Earth*, *119*, 8267–8282. https://doi.org/10.1002/2014JB011395

Hayward, N. J., & Ebinger, C. J. (1996). Variations in the along-axis segmentation of the Afar Rift system. *Tectonics*, *15*(2), 244–257. https://doi.org/10.1029/95TC02292

Illsley-Kemp, F., Keir, D., Bull, J. M., Gernon, T. M., Ebinger, C., Ayele, A., et al. (2018). Seismicity during continental breakup in the Red Sea rift of Northern Afar. *Journal of Geophysical Research: Solid Earth*, 123, 2345–2362. https://doi.org/10.1002/2017JB014902

Jónsson, S., & Xu, W. (2015). Volcanic eruptions in the southern Red Sea during 2007–2013. In N. M. A. Rasul, & I. C. F. Stewart (Eds.), *The Red Sea* (pp. 175–186). Berlin, Heidelberg: Springer Earth System Sciences.

Lundgren, P., Samsonov, S. V., López Velez, C. M., & Ordoñez, M. (2015). Deep source model for Nevado del Ruiz Volcano, Colombia, constrained by interferometric synthetic aperture radar observations. *Geophysical Research Letters*, *42*, 4816–4823. https://doi.org/10.1002/2015GL063858

Manighetti, I., Tapponnier, P., Courtillot, V., Gallet, Y., Jacques, E., & Gillot, Y. (2001). Strain transfer between disconnected, propagating rifts in Afar. *Journal of Geophysical Research*, *106*, 13,613–13,665. https://doi.org/10.1029/2000JB900454

Manighetti, I., Tapponnier, P., Gillot, P. Y., Jacques, E., Courtillot, V., Armijo, R., et al. (1998). Propagation of rifting along the Arabia–Somalia plate boundary: Into Afar. *Journal of Geophysical Research*, *103*(B3), 4947–4974. https://doi.org/10.1029/97JB02758

Mogi, K. (1958). Relations between the eruptions of various volcanoes and the deformations of the ground surfaces around them. *Bulletin Earthquake Research Institute, Tokyo*, *36*, 99–134.

Moore, C., Wright, T., Hooper, A., & Biggs, J. (2019). The 2017 Eruption of Erta 'Ale Volcano, Ethiopia: Insights into the shallow axial plumbing system of an incipient Mid-Ocean Ridge. *Geochemistry, Geophysics, Geosystems*, *20*, 5727–5743. https://doi.org/10.1029/2019GC008692

Nikkhoo, M., Walter, T. R., Lundgren, P. R., & Prats-Iraola, P. (2017). Compound dislocation models (CDMs) for volcano deformation analysis. *Geophysical Journal International*, *208*, 877–894. https://doi.org/10.1093/gji/ggw427

Nobile, A., Pagli, C., Keir, D., Wright, T. J., Ayele, A., Ruch, J., & Acocella, V. (2012). Dike-fault interaction during the 2004 Dallol intrusion at the northern edge of the Erta Ale Ridge (Afar, Ethiopia). *Geophysical Research Letters*, *39*, L19305. https://doi.org/10.1029/2012GL053152

Okada, Y. (1985). Surface deformation due to shear and tensile faults in a half-space. *Bulletin of the Seismological Society of America*, *75*, 1135–1154.

Pagli, C., Wright, T. J., Ebinger, C. J., Yun, S., Cann, J. R., Barnie, T., & Ayele, A. (2012). Shallow axial magma chamber at the slow-spreading Erta Ale Ridge. *Nature Geoscience*, *5*, 284–288. https://doi.org/10.1038/ngeo1414

Rivalta, E., & Segall, P. (2008). Magma compressibility and the missing source for some dike intrusions. *Geophysical Research Letters*, *35*, L04306. https://doi.org/10.1029/2007GL032521

Rosen, P. A., Gurrola, E., Sacco, G. F., & Zebker, H. (2012). *The InSAR Scientific Computing Environment* (pp. 730–733). Paper presented at Proceedings of the EUSAR, Nuremberg, Germany.

Segall, P. (2010). *Earthquake and volcano deformation* (p. 432). Princeton Univ. Press, N. J. https://doi.org/10.1515/9781400833856

Sigmundsson, F., Hreinsdóttir, S., Hooper, A., Árnadóttir, T., Pedersen, R., Roberts, M. J., et al. (2010). Intrusion triggering of the 2010 Eyjafjallajökull explosive eruption. *Nature*, *468*(7322), 426–430. https://doi.org/10.1038/nature09558

Tarasewicz, J., White, R. S., Woods, A. W., Brandsdottir, B., & Gudmundsson, M. T. (2012). Magma mobilization by downward-propagating decompression of the Eyjafjallajökull volcanic plumbing system. *Geophysical Research Letters*, *39*, L19309. https://doi.org/10.1029/2012GL053518

Tryggvason, E. (1984). Widening of the Krafla fissure swarm during the 1975-1981 volcano-tectonic episode. *Bulletin Volcanologique*, *47-1*, 47–69.

Valade, S., Ley, A., Massimetti, F., D'Hondt, O., Laiolo, M., Coppola, D., et al. (2019). Towards global volcano monitoring using multisensor sentinel missions and artificial intelligence: The MOUNTS monitoring system. *Remote Sensing*, *11*(13), 1528. https://doi.org/10.3390/rs11131528

Viltres, R., Jónsson, S., Ruch, J., Doubre, D., Reilinger, R., Floyd, M., & Ogubazghi, G. (2020). Kinematics and deformation of the southern Red Sea region from GPS observations. *Geophysical Journal International*, *221*, 2143–2154. https://doi.org/10.1093/gji/ggaa109

Williams, C. A., & Wadge, G. (2000). An accurate and efficient method for including the effects of topography in three-dimensional elastic models of ground deformation with applications to radar interferometry. *Journal of Geophysical Research*, *105*(B4), 8103–8120. https://doi.org/10.1029/1999JB900307

Wright, T. J., Ebinger, C., Biggs, J., Ayele, A., Yirgu, G., Keir, D., & Stork, A. (2006). Magma maintained rift segmentation at continental rupture in the 2005 Afar dyking episode. *Nature*, *442*, 291–294.

Xu, W., & Jónsson, S. (2014). The 2007–8 volcanic eruption on Jebel at Tair island (Red Sea) observed by satellite radar and optical images. *Bulletin of Volcanology*, *76*(2), 795. https://doi.org/10.1007/s00445-014-0795-9

Xu, W., Jónsson, S., Corbi, F., & Rivalta, E. (2016). Graben formation and dike arrest during the 2009 Harrat Lunayyir dike intrusion in Saudi Arabia: Insights from InSAR, stress calculations and analog experiments. *Journal of Geophysical Research: Solid Earth*, *121*, 2837–2851. https://doi.org/10.1002/2015JB012505

Xu, W., Rivalta, E., & Li, X. (2017). Magmatic architecture within a rift segment: Articulate axial magma storage at Erta Ale Volcano, Ethiopia. *Earth and Planetary Science Letters*, *476*, 79–86. https://doi.org/10.1016/j.epsl.2017.07.051

Xu, W., Ruch, J., & Jónsson, S. (2015). Birth of two volcanic islands in the southern Red Sea. *Nature Communications*, *6*(1), 7104. https://doi.org/10.1038/ncomms8104

Yu, C., Penna, N. T., & Li, Z. (2017). Generation of real-time mode high-resolution water vapor fields from GPS observations. *Journal of Geophysical Research: Atmospheres*, *122*, 2008–2025. https://doi.org/10.1002/2016JD025753